

# 3-D MODELLING OF A BILAYER HETEROJUNCTION ORGANIC SOLAR CELL BASED ON COPPER PHTHALOCYANINE AND FULLERENE (CUPC/C<sub>60</sub>): EVIDENCE OF TOTAL EXCITONS DISSOCIATION AT THE DONOR-ACCEPTOR INTERFACE

A. DIOUM, S. NDIAYE, E. H. O. GUÈYE, M. B. GAYE, D. N. FAYE, O. SAKHO, M. FAYE AND A. C. BEYE

(Received 11 October 2011; Revision Accepted 30 January 2012)

## ABSTRACT

A theoretical study of a 3-D modelled bilayer heterojunction organic photovoltaic cell based on copper phthalocyanine (CuPc) as electron donor and fullerene (C<sub>60</sub>) as electron acceptor is reported. The thin film multilayer stacking theory is applied to the bilayer heterojunction organic solar cell, with the optical matrix of the Abeles theory leading to new expression of generation rate and density of exciton photogenerated in the organic photoactive layer of CuPc/C<sub>60</sub>. The excitons density is investigated considering the excitons dissociation parameters at the different interfaces of the organic photoactive region, i.e. the exciton dissociation velocities  $S_{dp}$ ,  $S_{dg}$ ,  $S_{dj}$  and  $S_{dn}$  respectively associated to the transparent anode (ITO: Indium thin oxide)/donor (CuPc), the donor (CuPc)/acceptor (C<sub>60</sub>) and the acceptor (C<sub>60</sub>)/metallic cathode (Al: aluminium) interfaces. Moreover, the influences of the monochromatic light wavelength and the thickness  $w$  of the organic photoactive layer (CuPc/C<sub>60</sub>) on the exciton density are emphasized.

**KEYWORDS:** Bilayer Heterojunction - Organic Solar Cell – Exciton Dissociation

## 1. INTRODUCTION

Organic Solar Cells (OSC) are one of the most promising renewable and green energy sources due to their potential for low cost solar energy conversion, flexibility, large area capability and easy processing. So many efforts have been devoted to studying the mechanism of organic solar cells (OSC) conversion. The complexity of this system is exemplified by the various domains involved in its development, such as quantum mechanics, semiconductor physics, polymer science and chemistry. Several successful models based on various techniques of fabrication and modeling and/or characterization and simulation, have been developed to assess organic solar cell technology (Ameri *et al.*, 2009; Gonzalez-Valls *et al.*, 2009; Kippelen *et al.*, 2009; Krebs *et al.*, 2009; McNamara *et al.*, 2009; Monestier *et al.*, 2008; Nama *et al.*, 2010; Yi *et al.*, 2009; Yu *et al.*, 2010; Yang *et al.*, 2009; Wang *et al.*, 2010).

Nowadays, all the OSC have a planar layered structure, where the organic photoactive layer(s) is (are) sandwiched between two different electrodes. One is transparent i.e. a transparent conductive oxide (TCO) usually indium tin oxide (ITO), because it allows, up to now, to achieve better results. However, excellent works have been devoted to improve the influence of the TCO on the performance of the OSC (Bernède *et al.*, 2008). The other electrode is very often a metal such as silver (Ag) and aluminum (Al) which are very stable in air.

The first bilayer heterojunction OSC was studied by Tang (Tang, 1986). He used a heterojunction of copper phthalocyanine (CuPc) as electron donor and a perylene derivative (PV) as electron acceptor, improving the power conversion efficiency of OPV cell up to 1% which is higher than that of single layer cells efficiency. So many studies have been actively developed to improve the performance of OSC cells. The best results are obtained by vacuum co-sublimation of CuPc and C<sub>60</sub>

**A. Dioum**, Groupe de Physique de Solides et Sciences des Matériaux, Université Cheikh Anta Diop de Dakar, Sénégal

**S. Ndiaye**, Groupe de Physique de Solides et Sciences des Matériaux, Université Cheikh Anta Diop de Dakar, Sénégal

**E. H. O. Guèye**, Groupe de Physique de Solides et Sciences des Matériaux, Université Cheikh Anta Diop de Dakar, Sénégal

**M. B. Gaye**, Groupe de Physique de Solides et Sciences des Matériaux, Université Cheikh Anta Diop de Dakar, Sénégal

**D. N. Faye**, Groupe de Physique de Solides et Sciences des Matériaux, Université Cheikh Anta Diop de Dakar, Sénégal

**O. Sakho**, Groupe de Physique de Solides et Sciences des Matériaux, Université Cheikh Anta Diop de Dakar, Sénégal

**M. Faye**, Groupe de Physique Théorique, Département de Physique, Université Cheikh Anta Diop de Dakar, Sénégal

**A. C. Beye**, Groupe de Physique de Solides et Sciences des Matériaux, Université Cheikh Anta Diop de Dakar, Sénégal

(Monestier *et al.*, 2008; Peumans *et al.*, 2001; Yonehara *et al.*, 1996).

The mechanism of photocurrent production is explained as a result of initial generation of excitons by sunlight absorption, followed by diffusion of these excitons to the p-n interface and their dissociation into separated charge carriers (electrons and holes), which migrate to and are collected at the electrodes.

The local p-n interface geometry or morphology can have a positive impact on both exciton dissociation (which produces the photocurrent and needs to be maximized) and the recombination of charge transfer states formed after exciton dissociation (which decreases the photocurrent and needs to be minimized) (Yi *et al.*, 2009; McNamara *et al.*, 2009; Yonehara *et al.*, 1996).

Moreover different acceptors and donor have been tested. If  $C_{60}$  has been used with polymer, it has also been tested with organic molecular materials such as phthalocyanines (Pc). Copper phthalocyanine (CuPc), has been considered also with some perylene derivative. ITO/CuPc/Perylene derivative/Ag p-n junction cell showed 1% power conversion efficiency.

While a p-n junction is used for exciton dissociation, the absorption spectrum of the photosensitive layer, the p-type poly (3-butylthiophene), has been extended by adding a dye which absorbs in the visible region. The dye belongs to the indione group -PR3072- and a perylene derivative called MPP is used as n-type layer.

However, the best results have been obtained using multilayer structures based on the couple CuPc/ $C_{60}$ . However it can be already said that bilayer

structure allows achieving higher efficiency than single layer Schottky structure.

Peumans and Forrest have shown that after the introduction of a thin organic layer of bathocuproine (BCP) between the  $C_{60}$  and the cathode electrode a significant improvement of the cells performances is evidenced. With a device structure: ITO/PEDOT: PSS/CuPc/ $C_{60}$ /BCP/Al, a power energy efficiency of 3.6% has been measured. The BCP layer is called exciton-blocking layer (EBL), because it effectively blocks the diffusion of excitons to the cathode in such a way that such exciton confinement increases the probability of exciton dissociation at this interface (Yu *et al.*, 2009; Peumans *et al.*, 2001; Li *et al.*, 2009).

In order to improve the bilayer heterojunction OSC based on the couple CuPc/ $C_{60}$  performances, so many techniques of modeling and characterizing studies have been developed and others materials (Spanggaard *et al.*, 2004). In all the previous 1-D theoretical or experimental study, a hypothesis has been made on total exciton dissociation at the junction of the active layer, the measured experimental photocurrent being found consistent with such assumption (Yu *et al.*, 2009; McNamara *et al.*, 2009; Pettersson *et al.*, 1999).

This work presents a 3-D modeling of bilayer heterojunction organic solar cell based on copper phthalocyanine (CuPc) and a fullerene ( $C_{60}$ ). In our theoretical approach, evidence of the total exciton dissociation at the p-n junction is given, the exciton dissociation at the anode/donor and acceptor/cathode interfaces being negligible. The organic solar cell architecture under consideration is described as: **Anode (ITO)/PEDOT: PSS/CuPc/ $C_{60}$ /Alq<sub>3</sub>/cathode (Al)**.

#### where:

ITO: Indium Tin Oxide (100 nm)

PEDOT: PSS: Poly (3,4-ethylenedioxythiophène) doping Poly(4-styrenesulfonic acid) (80 nm)

CuPc: Copper phthalocyanine (50 nm)

$C_{60}$ : fullerene (50 nm)

Alq<sub>3</sub>: Aluminium tris (8-hydroxyquinolate) (1 nm)

Al: Aluminium (100 nm)

The schematic OSC architecture under consideration is presented in figure 1.

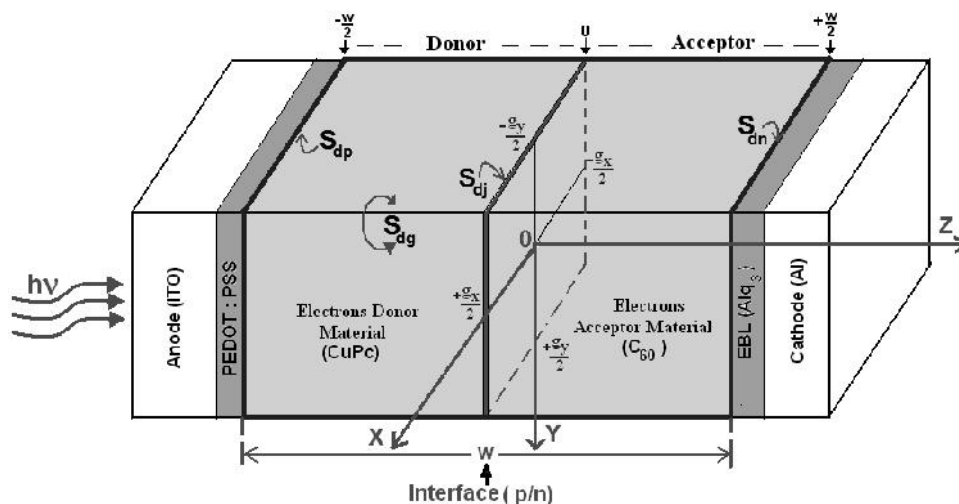


**Figure 1:** Scheme of a 3D bilayer heterojunction solar cell device based on CuPc/ $C_{60}$ .

By applying the thin film multilayer stacking theory on the organic solar cell, the optical matrix is obtained from Abeles method (Abelès 1950; Larivière *et al.*, 1992).

This allows to determine the optical (admittance, absorption, transmission) and electrical (power energy density, photon absorption rate, excitons

photogeneration rate) parameters of the cell. Then, excitons density photogenerated in the organic photoactive layer (CuPc/C<sub>60</sub>) is calculated by resolving the 3D-continuity equation relatively to the excitons diffusion. The total photocurrent density is deduced from this new expression of exciton density (Pettersson *et al.*,

1999; Stübinger *et al.*, 2001). Due to a MathCAD programme beforehand established, various profiles are obtained versus various variables such as the excitons dissociation velocities, the monochromatic light wavelength and the photoactive layer thickness.

## 2. THEORY

For modelling the 3D bilayer heterojunction OSC based on CuPc/C<sub>60</sub>, several assumptions have to be considered.

### 2.1. Assumptions

These assumptions are as follow:

- ✓ The different layers are homogenous and isotropic,
- ✓ The refraction (n) and extinction (k) indexes are in constant values and independent on layer thickness w,
- ✓ The interfaces are planes,
- ✓ The cross section is square with g<sub>x</sub>=g<sub>y</sub> (grain size),

The excitons dissociation velocities are materialized by the parameters S<sub>dp</sub>, S<sub>dg</sub>, S<sub>dj</sub> and S<sub>dn</sub>, respectively associated to the anode/donor, perpendicular boundaries surfaces to the plan of p/n junction /incidence area, donor/acceptor and acceptor/cathode interfaces.

The different excitons dissociation parameters chosen and defined as above are indicated in figure 1.

The highlighted region shown in figure 1 corresponds to the organic photoactive layer of the cell. Since, the different mechanisms of the photovoltaic conversion (photons absorption; excitons generation, diffusion and dissociation) are taking place in this region. Therefore, this study is limited to that region, and a Cartesian coordinate system (0,x,y,z) is then bound to and centred at the p-n junction interface of solar cell (red lines).

Hence, the figure 1 shows the different excitons dissociation velocity as:

- S<sub>dp</sub> is the excitons dissociation velocity at the anode (ITO)/donor (CuPc) interface,
- S<sub>dj</sub> is the excitons dissociation velocity at the donor (CuPc)/acceptor (C<sub>60</sub>) interface,
- S<sub>dn</sub> is the excitons dissociation velocity at the acceptor (C<sub>60</sub>)/metallic cathode (Alq<sub>3</sub>/Al) interface,
- S<sub>dg</sub> is the excitons dissociation velocity at the interfaces between the donor and acceptor surfaces perpendicular to the p/n junction and the incidence area as shown in figure 1.

The continuity equation established for our 3-D modelled bilayer heterojunction organic solar cell is then solved numerically in the following section.

## 2. 2. Computing Expressions

### 2. 2. 1. Continuity Equation

The continuity equation is given by the following expression in Eq. (1).

$$\frac{\partial^2 \dots_{exc}(x, y, z, \}, \}_{, \#)}{\partial x^2} + \frac{\partial^2 \dots_{exc}(x, y, z, \}, \}_{, \#)}{\partial y^2} + \frac{\partial^2 \dots_{exc}(x, y, z, \}, \}_{, \#)}{\partial z^2} - \frac{\dots_{exc}(x, y, z, \}, \}_{, \#)}{L_{exc}^2} = - \frac{G_{exc}(z, \#)}{D_{exc}} \quad (1)$$

where:  $\dots_{exc}(x, y, z, \}, \}_{, \#)$  is the global exciton density both photogenerated in the electrons n-type donor (CuPc) and p-type acceptor (C<sub>60</sub>) regions,  $D_{exc}$  the exciton diffusion coefficient,  $L_{exc}$  the exciton diffusion length,  $G(z, \#)$  the global generation rate both depending on spatial coordinate z (cell's depth) and  $\#$  the incidental angle diverging from the normal of the illuminated front side (anode), for any monochromatic light wavelength in the spectrum of visible.

In order to determine the excitons generation rate, we use the thin film multilayer stacking theory based on the optical and electrical properties of the cell study. In this approach, we take into account the transmission and reflection phenomena (interferential effects) due to the electromagnetic wave modulation in the various interfaces of the organic cell. This theory leads us to the optical matrix by using Abeles method.

Finally, the new expression of the excitons photogeneration rate is deduced from the optical matrix parameters as below:

$$G(z, \#) = \sum_{\} \frac{Q(z, \}, \#)}{\left( \frac{hc}{\} \right)} \quad (2)$$

where  $Q(z, \lambda, n)$  is the power energy density and defined as below:

$$Q(z, \lambda, n) = \frac{n}{n_0} r(\lambda) Q_{inc}(\lambda) \left| \frac{E(z, \lambda, n)}{E_{inc}} \right|^2 \quad (3)$$

$r(\lambda)$  is the absorption coefficient which depends on the monochromatic wavelength light and  $|E|$  is the module of the electric field.

The general solution of Eq.(1) can be expressed as below (Dugas, 1994):

$$\dots_{exc}(x, y, z, \lambda, n) = \sum_k \sum_j Z_{k,j}(z, \lambda, n) \cos(c_k x) \cos(c_j y) \quad (4)$$

where  $Z_{k,j}(z, \lambda, n)$  is a function of the depth which depends upon the z-variable. It can be obtained by combining the Eq.(4) and Eq.(1).

$$Z_{k,j}(z, \lambda, n) = A_{k,j}(\lambda, n) \cosh\left(\frac{z}{L_{k,j}}\right) + B_{k,j}(\lambda, n) \sinh\left(\frac{z}{L_{k,j}}\right) + \frac{1}{D_{k,j}} \frac{n_i}{n_0} \cdot \sum_{\lambda} \frac{I_{solaire}}{\left(\frac{hc}{\lambda}\right)} \cdot \frac{r(\lambda) e^{-r(\lambda) z \cos \theta}}{L_{k,j}^2 - r^2(\lambda) \cos^2 \theta} \quad (5)$$

with:

$$\frac{1}{D_{k,j}} = \frac{16 \sin\left(c_k \cdot \frac{g_x}{2}\right) \sin\left(c_j \cdot \frac{g_y}{2}\right)}{D_{exc} [c_k g_x + \sin(c_k \cdot g_x)] [c_j g_y + \sin(c_j \cdot g_y)]} \quad (6)$$

The coefficients  $A_{k,j}(\lambda, n)$ ,  $B_{k,j}(\lambda, n)$ ,  $c_k$  and  $c_j$  shown in this expression are given by the boundary conditions defined in the following paragraph and in the appendix.

### 2. 2. 1. 1. Boundary conditions

The boundary conditions are established to ensure that Eq. (1) has a single solution. Thus:

- At both interfaces:  $x = \pm \frac{g_x}{2}$

$$\left. \frac{\partial \dots_{exc}(x, y, z, \lambda, n)}{\partial x} \right|_{x=\pm \frac{g_x}{2}} = \pm \frac{S_{dg}}{D_{exc}} \dots_{exc}\left(\pm \frac{g_x}{2}, y, z, \lambda, n\right) \quad (7)$$

- At both interfaces:  $y = \pm \frac{g_y}{2}$

$$\left. \frac{\partial \dots_{exc}(x, y, z, \lambda, n)}{\partial y} \right|_{y=\pm \frac{g_y}{2}} = \pm \frac{S_{dg}}{D_{exc}} \dots_{exc}\left(x, \pm \frac{g_y}{2}, z, \lambda, n\right) \quad (8)$$

where  $S_{dg}$  is the exciton dissociation velocity in the interfaces ( $x = \pm \frac{g_x}{2}$ ,  $y = \pm \frac{g_y}{2}$ ).

- At the anode (ITO)/donor (CuPc) interface:  $z = -\frac{w}{2}$

$$\left. \frac{\partial \dots_{exc}(x, y, z, \lambda, n)}{\partial z} \right|_{z=-\frac{w}{2}} = + \frac{S_{dp}}{D_{exc}} \dots_{exc}\left(x, y, -\frac{w}{2}, \lambda, n\right)$$

- At the donor (CuPc)/acceptor (C<sub>60</sub>) interface or p/n junction:  $z = 0$

$$\left. \frac{\partial \dots_{exc}(x, y, z, \lambda, \mu)}{\partial z} \right|_{x=0^+} = + \frac{S_{dj}}{D_{exc}} \dots_{exc}(x, y, 0, \lambda, \mu) \quad (10)$$

- At the acceptor (C<sub>60</sub>)/cathode (Al) interface:  $z = + \frac{w}{2}$

$$\left. \frac{\partial \dots_{exc}(x, y, z, \lambda, \mu)}{\partial z} \right|_{x=+\frac{w}{2}} = - \frac{S_{dn}}{D_{exc}} \dots_{exc}\left(x, y, + \frac{w}{2}, \lambda, \mu\right) \quad (11)$$

where  $w$  is the photoactive organic layer (CuPc/C<sub>60</sub>) thickness,  $S_{dp}$ ,  $S_{dn}$  and  $S_{dj}$  are respectively the exciton dissociation velocities at the anode/donor, p/n and acceptor/cathode interfaces.

### 2. 2. 1. 2. Transcendental equations

By introducing the expression of the global excitons density (Eq. 4), in the boundary conditions (7) and (8), the  $c_k$  and  $c_j$  coefficients are obtained by solving the following transcendental equations:

- At the interface :  $x = \pm \frac{g_x}{2}$

$$\tan\left(c_k \frac{g_x}{2}\right) = \frac{S_{dg}}{D_{exc} c_k} \quad (12)$$

- At the interface :  $y = \pm \frac{g_y}{2}$

$$\tan\left(c_j \frac{g_y}{2}\right) = \frac{S_{dg}}{D_{exc} c_j} \quad (13)$$

By plotting the two transcendental equations in (12) and (13), the  $c_k$  and  $c_j$  values correspond to the intersection between the two curves of the first and second member of the transcendental equations. An example of such a transcendental equation graphical resolution is given in appendix 1.

The  $A_{k,j}(\lambda, \mu)$  and  $B_{k,j}(\lambda, \mu)$  constants of equations (4) and (5) are given by the boundary conditions (9), (10) and (11) and presented in appendix.

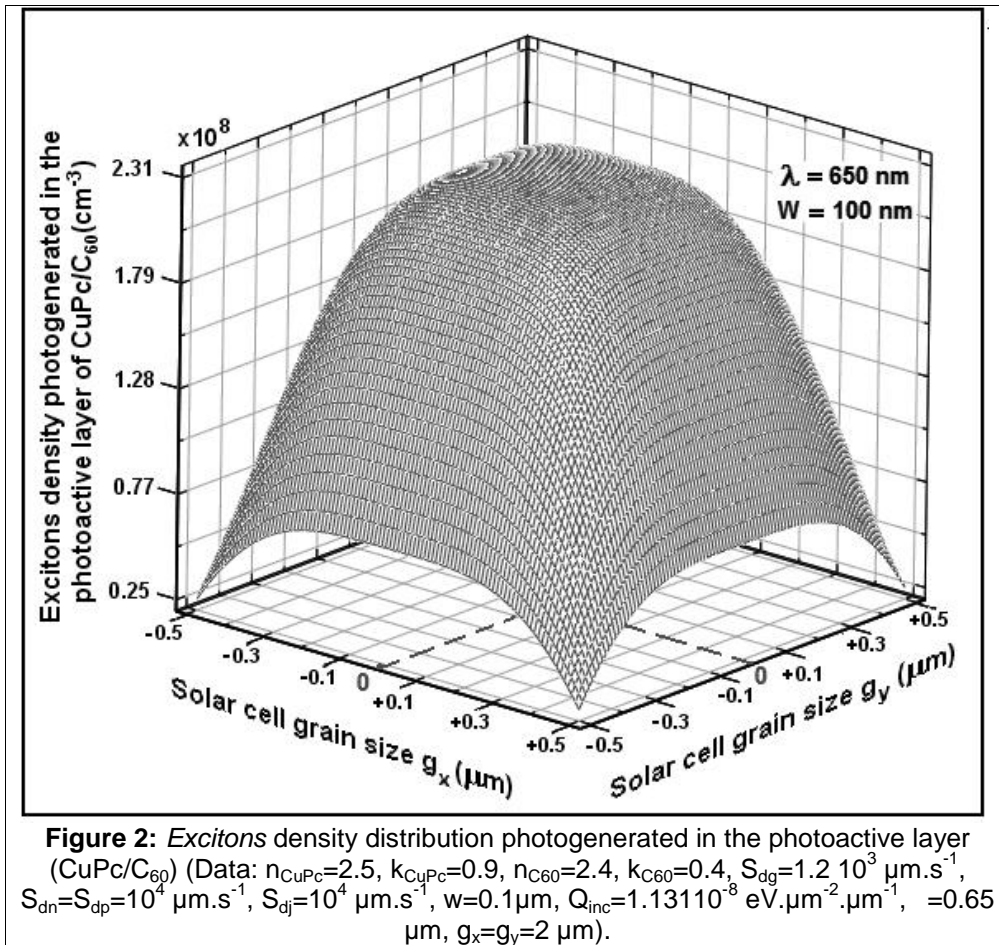
### 2. 3. Simulation results

The performance of an organic photovoltaic cell is related to the effectiveness of the excitons dissociation leading to the generation of free charge carriers at the

interfaces: anode/donor, p-n and acceptor/cathode, then transported to the electrodes where they are collected to contribute to the generation of photocurrent.

#### 2. 3. 1. Excitons density in the bulk of organic photoactive layer of CuPc/C<sub>60</sub>

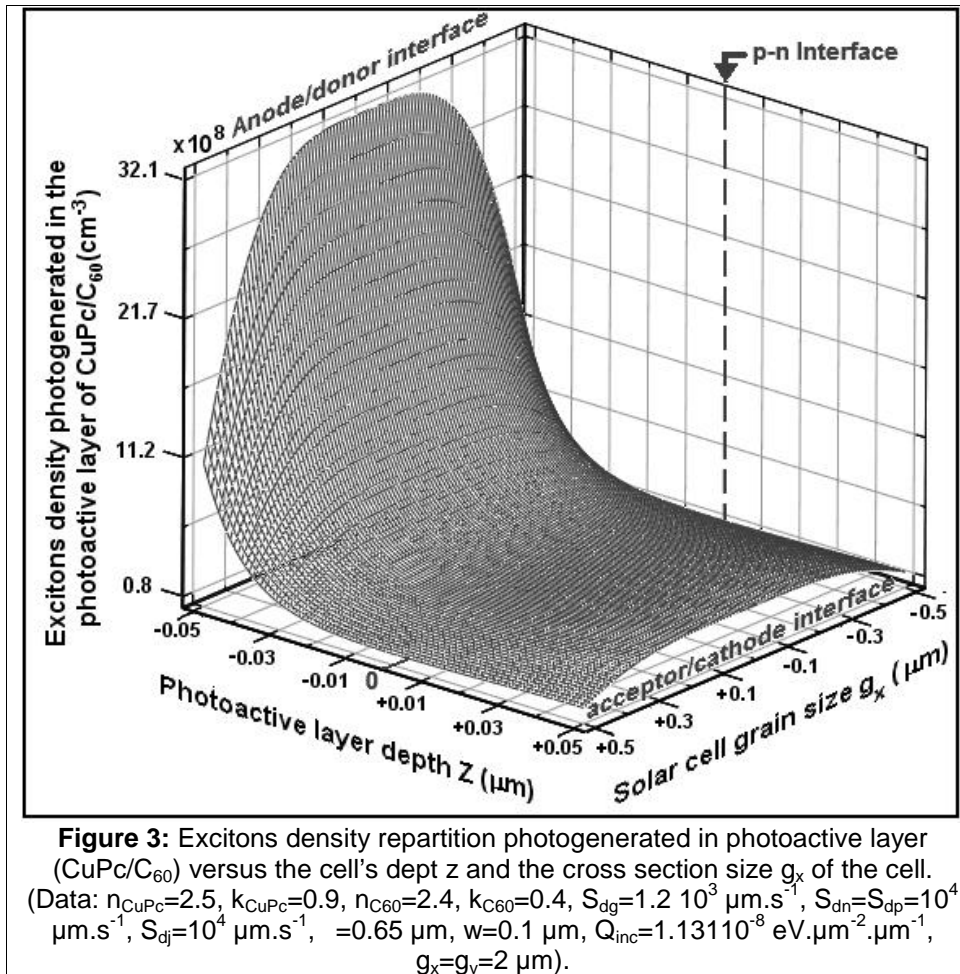
**Figure 2:** shows the excitons density distribution in the x- and y- directions of the CuPc/C<sub>60</sub> photoactive layer.



The excitons density photogenerated in the organic photoactive layer CuPc/C<sub>60</sub> presents a symmetrical distribution with respect to the z-axis perpendicular to the ( $g_x$ ,  $g_y$ ) plan of the p-n junction. This excitons distribution admits a maximum in the centre of the photoactive layer by presenting a stage (plate) parallelly to the p-n junction surface which corresponds to a null

gradient. Then the maximum corresponds to a strong excitons concentration which decreases when we move away from the centre towards the photoactive layer boundaries. In fact, excitons decrease in the boundaries would come from combined effects of excitons diffusion and then dissociation in the vicinity of the active interfaces.

**Figure 3:** displays the excitons density distribution in the CuPc/C<sub>60</sub> photoactive layer as a function of the depth z between  $-w/2$  and  $+w/2$  for a monochromatic radiation wavelength equal to 650 nm.

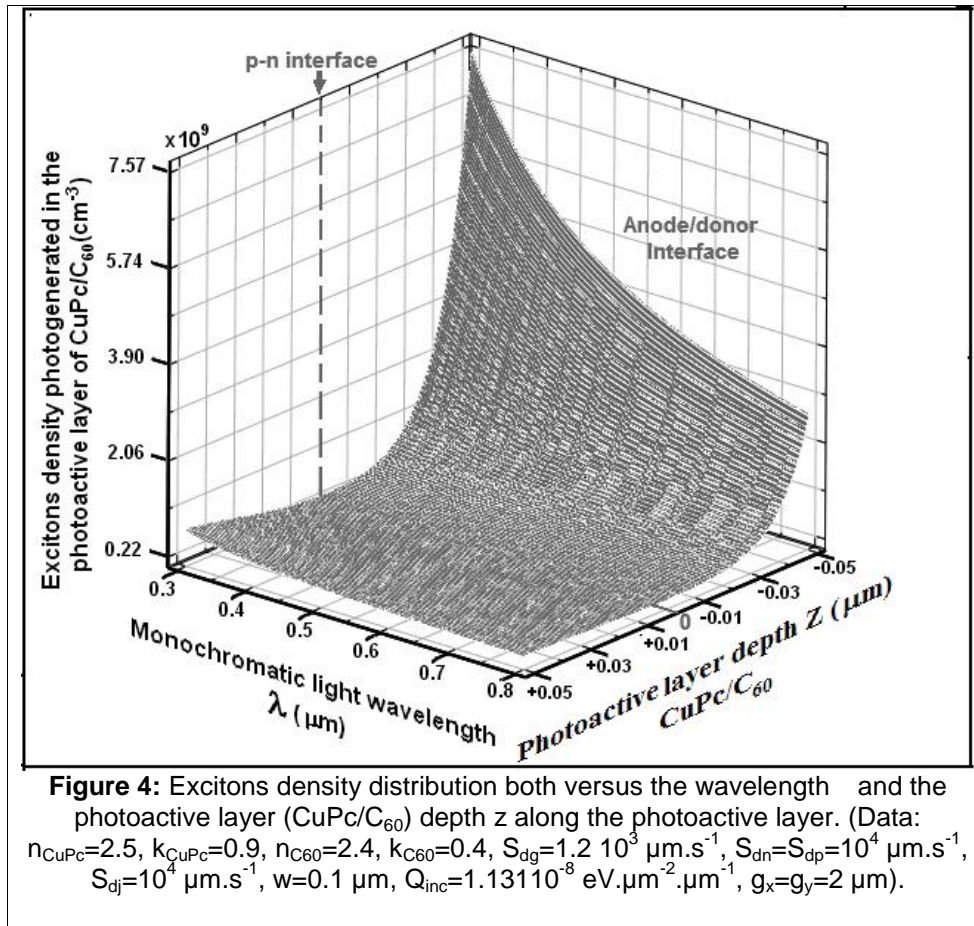


The density of the photogenerated excitons exhibit a maximum at the anode (ITO)/donor (CuPc) interface indicating that most of the excitons are created nearby the front surface. This density decreases very quickly until reaching a minimum quasi null near the p/n junction at  $z=0$ . Beyond the p/n junction, this density increases slightly towards the acceptor/cathode interface mostly as a result of exciton generation in this n-type region. As a matter of fact, exciton diffusion from the p-type side across the p-n junction and towards the acceptor/cathode interface is less likely. The weakness of the exciton density at this interface is a result of small

amount of photons reaching this area, most of the light being absorbed nearby the front surface.

However, a small increase of excitons photogenerated in the vicinity of the acceptor (C<sub>60</sub>)/cathode (Al) interface is due to the efficiency of the interfacial Exciton Blocking Layer but limited by the exciton dissociation. Actually, the EBL particularly the Alq<sub>3</sub> layer in this case is introduced between the electrons acceptor material (C<sub>60</sub>) and the metallic cathode (Al). Its role is both to reduce excitons diffusion towards this interface with the cathode even their dissociation in the very interface.

**Figure 4:** shows a decrease of the excitons density along the photoactive layer (CuPc/C<sub>60</sub>) depth z for any given monochromatic incidental light wavelength .



The same trend is also observed from shorter to longer wavelength in the the visible (400 - 800 nm) region. Indeed, we can note that, short wavelength of the visible are more favourable to excitons generation at the anode/donor interface ( $Z = -0.05 \mu\text{m}$ ). In fact, this phenomenon is foreseeable insofar as the CuPc admits two spectral regions of high absorption between the 300 - 400 nm and 500 - 700 nm.

## 2. 3. 2. Influence of exciton dissociation at the different actives interfaces

### 2. 3. 2. 1. At the donor (CuPc)/acceptor (C<sub>60</sub>) interface or p-n junction

The exciton density photogenerated in the photoactive layer CuPc/C<sub>60</sub> is plotted a function of the exciton dissociation velocity  $S_{\text{dj}}$  at the donor/acceptor interface (or p-n junction) respectively for different incident monochromatic wavelength (figure 5) and for different values of the photoactive layer thickness  $w$  (figure 6).

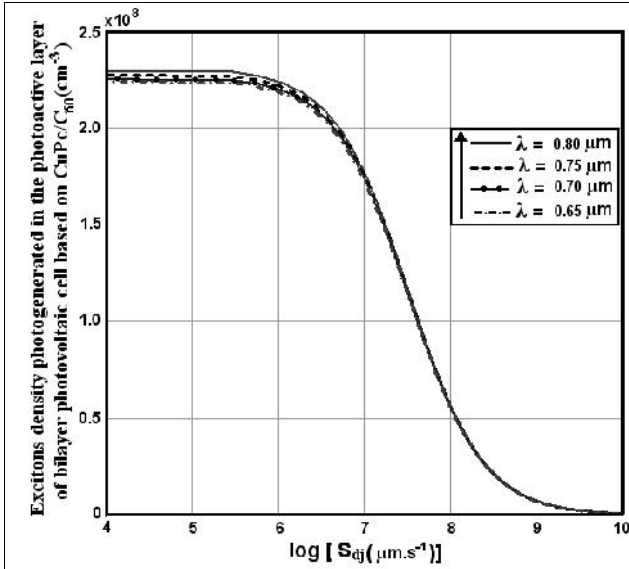


**Figure 5:** Excitons density photogenerated in the CuPc/C<sub>60</sub> layer versus the logarithmic of exciton dissociation velocity  $S_{dj}$  at the p-n junction for different values of the monochromatic light wavelength. (Data :  $n_{CuPc}=2.5$ ,  $k_{CuPc}=0.9$ ,  $n_{C60}=2.4$ ,  $k_{C60}=0.4$ ,  $S_{dg}=1.2 \cdot 10^3 \mu\text{m}\cdot\text{s}^{-1}$ ,  $S_{dn}=10^4 \mu\text{m}\cdot\text{s}^{-1}$ ,  $S_{dp}=10^4 \mu\text{m}\cdot\text{s}^{-1}$ ,  $Q_{inc}=1.13110^{-8} \text{ eV}\cdot\mu\text{m}^{-2}\cdot\mu\text{m}^{-1}$ ,  $g_x=g_y=2 \mu\text{m}$ .)

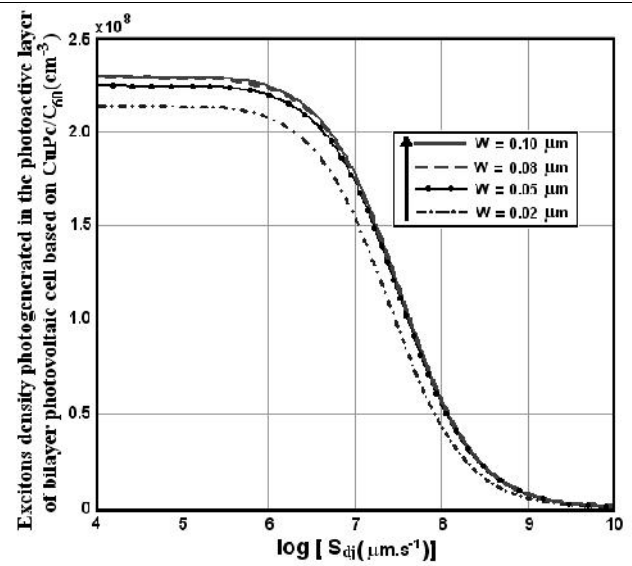


**Figure 6:** Exciton density photogenerated in the CuPc/C<sub>60</sub> layer versus the logarithmic of exciton dissociation velocity  $S_{dj}$  at the p-n junction for different values of the photoactive layer thickness  $w$ . (Data :  $n_{CuPc}=2.5$ ,  $k_{CuPc}=0.9$ ,  $n_{C60}=2.4$ ,  $k_{C60}=0.4$ ,  $S_{dg}=1.2 \cdot 10^3 \mu\text{m}\cdot\text{s}^{-1}$ ,  $S_{dn}=10^4 \mu\text{m}\cdot\text{s}^{-1}$ ,  $S_{dp}=10^4 \mu\text{m}\cdot\text{s}^{-1}$ ,  $Q_{inc}=1.13110^{-8} \text{ eV}\cdot\mu\text{m}^{-2}\cdot\mu\text{m}^{-1}$ ,  $g_x=g_y=2 \mu\text{m}$ .)

The photogenerated-exciton density presents a null gradient which remains constant from low exciton-dissociation velocity  $S_{dj}$  up to  $10^6 \text{ m}\cdot\text{s}^{-1}$ . Then it decreases exponentially until reaching a quasi null value approximately for exciton-dissociation velocity  $S_{dj}$  of about  $10^9 \text{ m}\cdot\text{s}^{-1}$ . Indeed, the effectiveness of exciton dissociation  $S_{dj}$  at the p-n junction is induced by an internal electric field one and in the other hand by a charge transfer between the donor and acceptor materials. Although weak, the exciton density decreases with the monochromatic light wavelength (figure 5). It increases very appreciably with the thickness  $w$  and is

recombination-limited for  $w$  far beyond the exciton diffusion length (figure 6).

### 2. 3. 2. 2. Dissociation at the anode (ITO)/donor (CuPc) and at the acceptor (C<sub>60</sub>)/cathode (Al) interfaces

In order to check the competitive role of the exciton dissociation velocities  $S_{dj}$ ,  $S_{dp}$  and  $S_{dn}$  at the various active interfaces, respectively at the p-n junction, the anode/donor and the acceptor/cathode, the exciton density photogenerated in the photoactive layer CuPc/C<sub>60</sub> is plotted in figures 7 and 8 as a function of  $S_{dj}$  for different values of  $S_{dp}$  and  $S_{dn}$ .

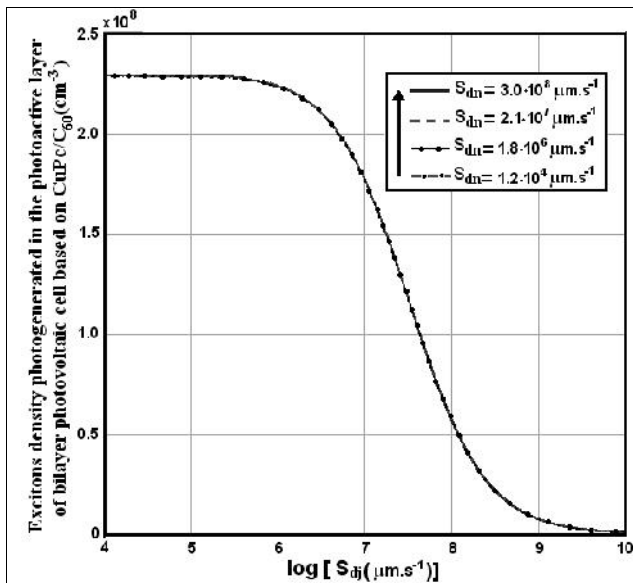


**Figure 7:** Exciton density photogenerated in the CuPc/C<sub>60</sub> layer versus the logarithmic of exciton dissociation velocity  $S_{dj}$  at the p-n junction for different values of exciton dissociation velocity  $S_{dn}$  at the acceptor/cathode interface (Data:  $n_{CuPc}=2.5$ ,  $k_{CuPc}=0.9$ ,  $n_{C60}=2.4$ ,  $k_{C60}=0.4$ ,  $\lambda=0.65 \mu m$ ,  $S_{dg}=1.2 \cdot 10^3 \mu m.s^{-1}$ ,  $w=0.1 \mu m$ ,  $Q_{inc}=1.13110^{-8} eV.\mu m^{-2}.\mu m^{-1}$ ,  $g_x=g_y=2 \mu m$ ).

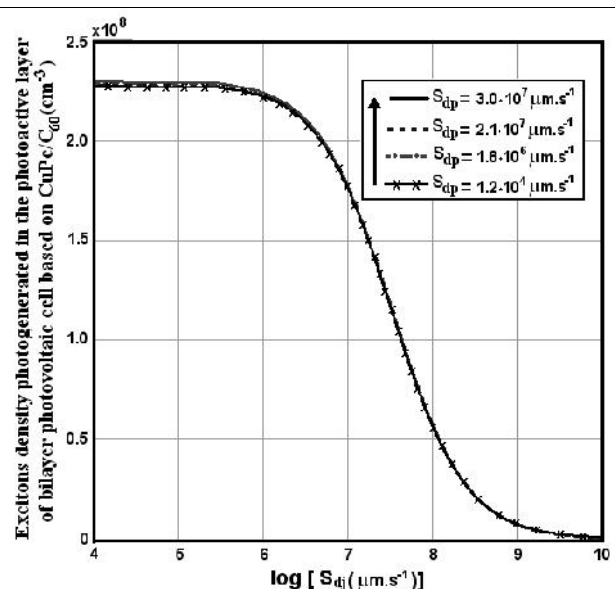


**Figure 8:** Exciton density photogenerated in the CuPc/C<sub>60</sub> layer versus the logarithmic of exciton dissociation velocity  $S_{dj}$  at the p-n junction for different values of exciton dissociation velocity  $S_{dp}$  at the anode/donor interface. (Data:  $n_{CuPc}=2.5$ ,  $k_{CuPc}=0.9$ ,  $n_{C60}=2.4$ ,  $k_{C60}=0.4$ ,  $\lambda=0.65 \mu m$ ,  $S_{dg}=1.2 \cdot 10^3 \mu m.s^{-1}$ ,  $w=0.1 \mu m$ ,  $Q_{inc}=1.13110^{-8} eV.\mu m^{-2}.\mu m^{-1}$ ,  $g_x=g_y=2 \mu m$ ).

Any variation of about three to four orders of magnitude (from  $10^4 m.s^{-1}$  to  $10^8 m.s^{-1}$ ) of the exciton dissociation velocities  $S_{dp}$  and  $S_{dn}$  does not affect at all dependence of the photogenerated-exciton density on  $S_{dj}$ . This consequently gives striking evidence that the exciton dissociation at the p-n junction plays the major role in charge carriers and then photocurrent generation.

### 3. DISCUSSION

Previously, many studies have been devoted to excitons photogenerated which of treatment is not included in modelling of organic solar cell. Then, excitons should be taken into account because of very essential producing free charge carriers (electron, hole). Actually, the photocurrent output and efficiency of organic solar cell production depend on excitons dissociation.

In all published papers such as Monestier et al model are in one dimension and total exciton dissociation at the donor/acceptor interface of bilayer heterojunction organic solar cell based on CuPc/C<sub>60</sub> has been assumed. Otherwise, Burgelman et al. are extended Green and Zhang modelling by including exciton dissociation either at an interface, or in the bulk or in the space charge layer (SCL) of organic solar cell.

By using theoretical tool such as thin film stacking and Abeles theory, our model clearly demonstrated for the first time:

- ✓ Evidence of the efficient exciton dissociation at the p-n junction or donor/acceptor.
- ✓ 3D modelling study to determine new expression of excitons density photogenerated in the CuPc/C<sub>60</sub> organic layer and exciton photogeneration rate.

- ✓ Introduction of new parameters of excitons dissociation velocity assumed to the different surface and to the p-n junction or donor /acceptor interface.

### 4. CONCLUSION

Theoretical study is made on bilayer heterojunction organic solar cell based on copper phthalocyanine (CuPc/C<sub>60</sub>) versus exciton dissociation velocities at the different interfaces of the organic photoactive layer. Evidence of total dissociation of excitons at the p-n junction is given while the exciton dissociations at the anode/donor and the acceptor/cathode interfaces are found negligible.

These results confirm and justify the assumption extensively made in the literature that the main part of the free charge carriers result from exciton dissociation at the p-n junction or donor/acceptor interface. This opened the way for a 3D-modelling, computing of the photocurrent density and the operating points of the bilayer heterojunction organic solar cell.

### ACKNOWLEDGMENTS:

The authors wish to thank the World Federation of Scientists for its financial support through a 2009-2010 and 2010-2011 fellowship granted the thesis of Dr Dioum.

### REFERENCES:

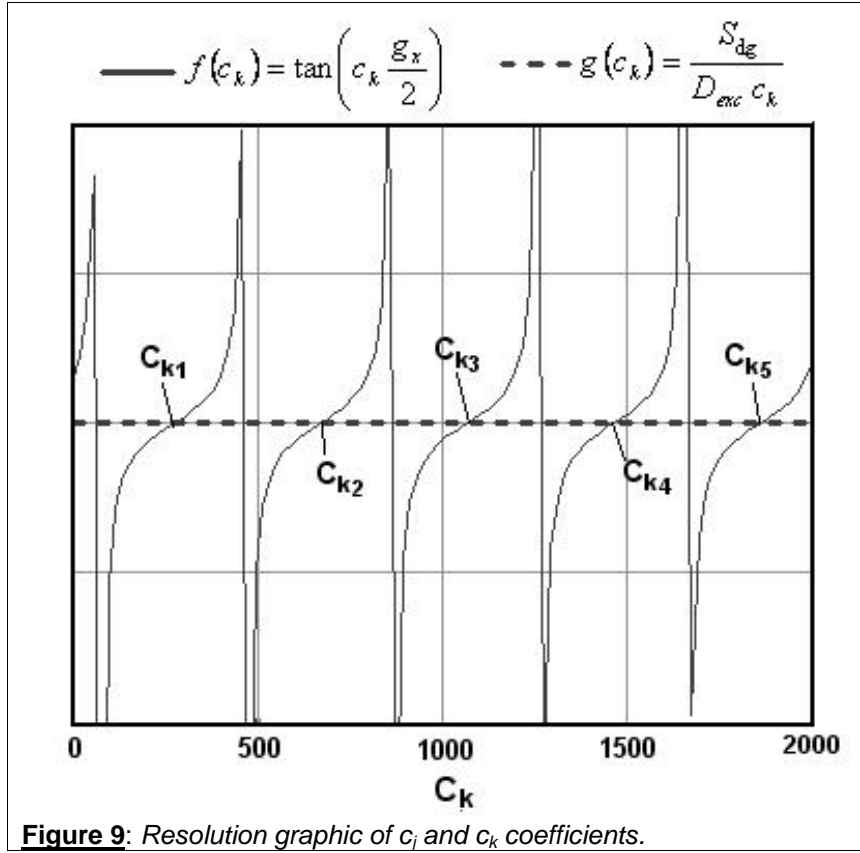
- Abelès, F., 1950. Recherches sur la propagation des ondes électromagnétiques sinusoïdales dans les milieux stratifiés. Ann. Phys. Ser. (12): 706.

- Ameri, T., Dennler, G., Lungenschmied, C and Brabec, C. J., 2009. Organic tandem solar cells: a review. *Energy Environ. Sci.* (2): 347–363.
- Bernède, J. C., Berredjem, Y., Cattin, L and Morsli, M., 2008. Improvement of organic solar cell performances using a zinc oxide anode coated by an ultrathin metallic layer, *Applied Physics Letters* (92): 083304.
- Burgelman, M and Minnaert, B., 2006. Including excitons in semiconductor solar cell modeling. *Thin Solid Films* (511-512): 214-218.
- Dugas, J., 1994. 3D modelling of a reverse cell made with improved multicrystalline silicon wafers. *Solar Energy Materials and Solar Cells* (32): 71-88.
- Gonzalez-Valls, I and Lira-Cantu, M., 2009. Vertically-aligned nanostructures of ZnO for excitonic solar cells: a review. *Energy Environ. Sci.* (2): 19–34.
- Gunes, S., Neugebauer, H and Sariciftci, N. S., 2007. Conjugated polymer-based organic solar cells. *Chem. Rev.* (107): 1324–1338.
- Kippelen, B and Brédas, J. L., 2009. Organic photovoltaics. *Energy Environ. Sci.* (2): 251-261
- Krebs, F. C., 2009. Fabrication and processing of polymer solar cells: a review of printing and coating techniques. *Sol. Energy Mater. Sol. Cells* (93): 394–412.
- McNamara, A., Seering, J and Zeng, Y., 2009. Model and Optimization of Organic Photovoltaic Cells, Institute for Mathematics and its Applications at the University of Minnesota. IMA Interdisciplinary REU. USA, 20.
- Monestier, F., Simon, J. J., Torchio, P., Escoubas, L., Ratier, B., Hojeij, W., Lucas, B., Moliton, A., Cathelinaud, M., Defranoux, C and Flory, F., 2008. Optical modeling of organic solar cells based on CuPc and C<sub>60</sub>. *Applied Optics* 47 (13): 251-256.
- Nama, Y. M., Huh, J and Jo, W. H., 2010. Optimization of thickness and morphology of active layer for high performance of bulk-heterojunction organic solar cells. *Solar Energy Materials & Solar Cells* (94): 1118–1124.
- Ning Li, Brian E. Lassiter, Richard R. Lunt, Guodan Wei, and Stephen R. Forrest, 2009. Open circuit voltage enhancement due to reduced dark current in small molecule photovoltaic cells. *Applied Physics Letters*, (94): 0233307.
- Parjadis de Larivière, G., Frigerio, G. M., Rivory, J and Abelès, F., 1992. Estimate of the degree of inhomogeneity of the refractive index of dielectric films from spectroscopic ellipsometry. *Appl. Optics* 31, (28): 6056-6060.
- Pettersson, L. A. A., Roman, L.S and Inganäs, O., 1999. Modeling photocurrent action spectra of photovoltaic devices based on organic thin films. *Journal of Applied Physics* (86): 487.
- Peumans, P and Forrest, S. R., 2001. Very-high-efficiency double-heterostructure copper phthalocyanine/C<sub>60</sub> photovoltaic cells. *Appl. Phys. Lett* (79): 126.
- Spanggaard, H and Krebs, F. C., 2004. A brief history of the development of organic and polymeric photovoltaics. *Solar Energy Materials & Solar Cells* 83, (2-3): 125-146.
- Stübinger, T and Brütting, W., 2001. Exciton diffusion and optical interference in organic donor–acceptor photovoltaic cells. *Journal of Applied Physics*, 90, (7): 3632.
- Tang, C. W., 1986. Two layer organic photovoltaic cell. *Appl. Phys. Lett.* 48, (2): 183-185.
- Yang, Y and Wudl, F., 2009. Organic Electronics: From Materials to Devices. *Advanced Materials* 21, (14-15): 1401-1403.
- Yi, Y., Coropceanu, V and Brédas, J. L., 2009. Exciton-Dissociation and Charge-Recombination Processes in Pentacene/C<sub>60</sub> Solar Cells: Theoretical Insight into the Impact of Interface Geometry. *J. Am. Chem. Soc.* (131): 15777–15783.
- Yonehara, H and Pac, C., 1996. Photoelectrical properties of double-layer organic solar cells using C<sub>60</sub> and phthalocyanines. *Thin Solid Films*, (278): 108-113.
- Yu, J., Huang, J., Lin, H and Jiang, Y., 2010. Exciton diffusion length analysis of mixed donor materials in organic solar cells by doping with phosphorescent iridium complex. *J. Appl. Phys.* (108): 113111.
- Yu, J. S., Huang, Zhang, J., L and Jiang, Y. D., 2009. Energy losing rate and open-circuit voltage analysis of organic solar cells based on detailed photocurrent simulation. *J. Appl. Phys.* (106): 063103.
- Wang, N., Yu, J., Lin, H and Jiang, Y., 2010. Organic Photovoltaic Cells with Improved Performance Using Bathophenanthroline as a Buffer Layer. *Chin. J. Chem. Phys.* 23, (1):84-88.

## APPENDIX:

## 1. Transcendental equations resolution

In this paragraph we present an example of resolution of transcendental equation. This is a graphical resolution which allows us obtaining the different  $c_i$  and  $c_k$  coefficient values met in the exciton density expression (figure 9).



The  $c_i$  and  $c_k$  values correspond to the intersection between the two curves: one in continue line (red line) which corresponds to the first member the transcendental equation and other in discontinue line (blue line) which corresponds to second member of the transcendental equation.

## 2. Expressions of the constants

The constants  $A_{k,j}(\lambda, n)$  and  $B_{k,j}(\lambda, n)$  are given by the boundaries conditions (9), (10) and (11). Their expressions are computed and take the different shape defined as below:

- For p-type (CuPc):  $z = -\frac{w}{2}$

$$A_{kjp} = -\sum_{\lambda} a_{kjex} \cdot \left( \frac{\left( \frac{S_{dj}}{D_{exc}} - r(\lambda) \cdot \cos(n) \right) \cdot X_{kjp} + \frac{1}{L_{kjex}} \cdot \left( \frac{S_{dp}}{D_{exc}} + r(\lambda) \cdot \cos(n) \right) \cdot \exp(+w_p \cdot r(\lambda) \cdot \cos(n))}{\frac{S_{dj}}{D_{exc}} \cdot X_{kjp} + \frac{1}{L_{kjex}} \cdot Y_{kjp}} \right) \quad (14)$$

$$B_{kjp} = \sum_{\lambda} a_{kjex} \cdot \left( \frac{\left( \frac{S_{dp}}{D_{exc}} \right) \cdot \left( \frac{S_{dp}}{D_{exc}} + r(\lambda) \cdot \cos(n) \right) \cdot \exp(+w_p \cdot r(\lambda) \cdot \cos(n)) - \left( \frac{S_{dj}}{D_{exc}} - r(\lambda) \cdot \cos(n) \right) \cdot Y_{kjp}}{\frac{S_{dj}}{D_{exc}} \cdot X_{kjp} + \frac{1}{L_{kjex}} \cdot Y_{kjp}} \right) \quad (15)$$

- For n-type ( $C_{60}$ ):  $z = +\frac{w}{2}$

$$A_{kjin} = -\sum_{\lambda} a_{kjex} \cdot \frac{\left(\frac{S_{dj}}{D_{exc}} + r(\lambda) \cdot \cos(\mu)\right) \cdot X_{kjin} + \frac{1}{L_{kjex}} \cdot \left(\frac{S_{dn}}{D_{exc}} - r(\lambda) \cdot \cos(\mu)\right) \cdot \exp(-w_n \cdot r(\lambda) \cdot \cos(\mu))}{\frac{S_{dj}}{D_{exc}} \cdot X_{kjin} + \frac{1}{L_{kjex}} \cdot Y_{kjin}} \quad (16)$$

$$B_{kjin} = -\sum_{\lambda} a_{kjex} \cdot \frac{\left(\frac{S_{dj}}{D_{exc}} + r(\lambda) \cdot \cos(\mu)\right) \cdot Y_{kjin} - \left(\frac{S_{dn}}{D_{exc}}\right) \cdot \left(\frac{S_{dn}}{D_{exc}} - r(\lambda) \cdot \cos(\mu)\right) \cdot \exp(-w_n \cdot r(\lambda) \cdot \cos(\mu))}{\frac{S_{dj}}{D_{exc}} \cdot X_{kjin} + \frac{1}{L_{kjex}} \cdot Y_{kjin}} \quad (17)$$

with

$$X_{kjp} = \frac{1}{L_{kj}} \cosh\left(\frac{w_p}{L_{kj}}\right) + \frac{S_{dp}}{D_{exc}} \sinh\left(\frac{w_p}{L_{kj}}\right) \quad (18)$$

$$Y_{kjp} = \frac{1}{L_{kj}} \sinh\left(\frac{w_p}{L_{kj}}\right) + \frac{S_{dp}}{D_{exc}} \cosh\left(\frac{w_p}{L_{kj}}\right) \quad (19)$$

$$X_{kjin} = \frac{1}{L_{kj}} \cosh\left(\frac{w_p}{L_{kj}}\right) + \frac{S_{dn}}{D_{exc}} \sinh\left(\frac{w_p}{L_{kj}}\right) \quad (20)$$

$$Y_{kjin} = \frac{1}{L_{kj}} \sinh\left(\frac{w_p}{L_{kj}}\right) + \frac{S_{dn}}{D_{exc}} \cosh\left(\frac{w_p}{L_{kj}}\right) \quad (21)$$